

Article

GIS-Based Detection of Gullies in Terrestrial LiDAR Data of the Cerro Llamoca Peatland (Peru)

Bernhard Höfle ^{1,*}, Luisa Griesbaum ¹ and Markus Forbriger ²

¹ Institute of Geography & Heidelberg Center for the Environment (HCE), University of Heidelberg, D-69120 Heidelberg, Germany; E-Mail: L.Griesbaum@stud.uni-heidelberg.de

² Institute of Geography, University of Cologne, D-50932 Cologne, Germany; E-Mail: m.forbriger@uni-koeln.de

* Author to whom correspondence should be addressed; E-Mail: hoefle@uni-heidelberg.de; Tel.: +49-6221-54-5594; Fax: +49-6221-54-4529.

Received: 19 August 2013; in revised form: 31 October 2013 / Accepted: 1 November 2013 / Published: 11 November 2013

Abstract: Cushion peatlands are typical features of the high altitude Andes in South America. Due to the adaptation to difficult environmental conditions, they are very fragile ecosystems and therefore vulnerable to environmental and climate changes. Peatland erosion has severe effects on their ecological functions, such as water storage capacity. Thus, erosion monitoring is highly advisable. Erosion quantification and monitoring can be supported by high-resolution terrestrial Light Detection and Ranging (LiDAR). In this study, a novel Geographic Information System (GIS)-based method for the automatic delineation and geomorphometric description of gullies in cushion peatlands is presented. The approach is a multi-step workflow based on a gully edge extraction and a sink filling algorithm applied to a conditioned digital terrain model. Our method enables the creation of GIS-ready polygons of the gullies and the derivation of geomorphometric parameters along the entire channel course. Automatically derived boundaries and gully area values correspond to a high degree (93%) with manually digitized reference polygons. The set of methods developed in this study offers a suitable tool for the monitoring and scientific analysis of fluvial morphology in cushion peatlands.

Keywords: LiDAR; terrestrial laser scanning; GIS; gully detection; geomorphometry; peatland

1. Introduction

Being strongly connected to climate and land use change, gully and soil erosion are an increasing problem causing major socio-economic impacts and significant loss of sediments exiting agricultural landscapes [1]. Soil degradation requires monitoring and a full understanding of the processes and complex interrelated systems, especially in highly sensitive ecosystems [2]. Cushion peatlands are typical elements of the high Andean vegetation zones and important ecosystems due to their water storage capacity in the mostly semiarid to arid Puna. Through rivers they also supply oases in the hyperarid coastal desert in Peru and Chile. Hence, cushion peatlands are part of the local people's livelihood as they are used as pasture and water reservoirs, and are therefore important for agriculture [2,3]. In these naturally regulated ecosystems, mostly anthropogenic intervention causes gully erosion and, thus, leads to degradation and desiccation [2,4].

Studies on gully erosion take place mostly in semi-arid regions, since erosion mainly occurs due to sparse vegetation cover and sporadic but often heavy rainfall. Background information about characteristics, processes and morphology of gullies is found in [1,5–7]. Although water erosion is not a typical process in peatlands, it is observed in various upland peats [8–10]. The studies of [2,3] provide more detailed information on these typical landforms of the Andean highland and [4] gives insights particularly into the Llamoca peatland in Peru, the study area of this research.

Area-wide erosion monitoring and quantification in peatlands is made possible by applying remote sensing to collect detailed 3D topographic information and to derive digital elevation models (DEMs). DEMs are input to GIS-based geomorphometric analysis and the implementation of erosion models [11]. First, to generate such a submeter resolution DEM adequate data sources are necessary. Second, to identify the affected landscape in the DEM dataset, geomorphological landform mapping through feature detection algorithms is required.

LiDAR, also referred to as laser scanning, provides reliable and accurate 3D point clouds, from which high-resolution Digital Terrain Models (DTMs) can be derived for geomorphological studies [12,13]. The DTM represents a DEM of the bare Earth without elevated anthropogenic objects and high vegetation. In particular ground-based LiDAR, *i.e.*, Terrestrial Laser Scanning (TLS), offers high point densities to derive submeter resolution DTMs. TLS is applied for the investigation of landforms with small spatial extent and processes with low magnitudes of changes over time [14–16]. Additionally, TLS is a suitable field method to derive DTMs in areas where high precision airborne acquisition is hampered due to difficult flight conditions (e.g., high altitude, wind conditions) or costs. Furthermore, in gully research TLS is often used as high quality reference dataset to evaluate different field methods for quantifying gully erosion in 2D and 3D (e.g., eroded gully volume) [17,18].

The quality of LiDAR-derived DTMs—in terms of DTM resolution, vertical and horizontal elevation accuracy—enables automatic detection of detailed natural landforms as well as man-made objects [19]. Automatic GIS classifications are usually based on morphometric characteristics, such as slope, curvature, aspect, or other derivatives of elevation [13,20,21]. Gully detection is of high importance regarding erosion monitoring and gully erosion modeling, which aims at predicting erosion rates and the impact of gully development, e.g., on hydrology and sediment budgets [22].

The aim of our study is to present and examine the potential of a new GIS-based workflow for detecting gullies in cushion peatlands from TLS DTMs. Utilization of TLS data coupled with GIS

enabling automatic gully detection is still underexploited (Section 2). Former works on gully detection concentrated mostly on the extraction of linear features to form gully networks. In contrast, this work aims at mapping gully erosion areas as polygons, which enables straightforward volumetric and multitemporal analysis of changes in morphology over time. The study area is located in the catchment area of Río Viscas at the foot of Cerro Llamoca, Peru (Section 3). Due to the high altitude of the catchment (~4400 m a.s.l.), and its remote location, no detailed elevation information of the micro-topography has been available previous to this investigation. The objects of interests are gullies with a dimension of a few meters up to more than 50 m in width. In this study, we demonstrate for the first time the utilization of TLS for geomorphological mapping of gullies in high altitude Andean cushion peatlands for a relatively large study extent with almost 2 km² (Section 4). The results are compared with gully outlines digitized manually by several geomorphologists (Section 5).

Apart from the methodological progress in this paper, we expect to stimulate research on cushion peatlands using LiDAR and GIS, which will help to enhance the understanding of the underlying geomorphological processes, channel response and catchment behavior including gully erosion and hydrology.

2. Related Works

Previous works mainly used satellite or aerial images for mapping of gullies. GIS-based gully monitoring using high-resolution (<0.1 m) aerial photography taken from blimp and kite platforms are performed in the study of [23]. The monitoring over several years of two gullies located in Spain yields the capability of deriving DEMs from this data source. However, vegetation cover and the specific morphology of the gullies make fully automatic DEM derivation difficult. In [24] IKONOS and GEOEYE-1 satellite images are used as input of an object-based image analysis (OBIA) for mapping of the gully system area in a study site in Morocco. Input features for segmentation and classification are derived from topographic, spectral, shape and contextual information. They generate a 1m-DTM from a Digital Surface Model (DSM) derived from a GEOEYE-1 stereo-pair, from which features such as slope, flow direction, specific catchment area, *etc.*, are derived. The detected gully system area differs only slightly (<2%) from the reference area. In the study of [25] a multi-scale OBIA approach is developed using unmanned aerial vehicle (UAV) photographs as an input layer where image (RGB) contrast information and shape properties of segments are considered. The OBIA workflow includes a multi-resolution segmentation and knowledge-based classification designed for the investigated landform. Compared with manually detected reference landforms, gully mapping achieves detection rates of around 67%.

Recent studies make use of LiDAR data predominantly obtained from airborne platforms [13]. In particular, LiDAR can enable geomorphological mapping of vegetated areas where passive remote sensing techniques do not provide sufficient ground information below high vegetation (e.g., [26]). GIS-based geomorphological mapping by means of airborne LiDAR data for landform identification and delineation has been used for several years such as for fluvial morphological landforms [27,28] and quantification of multitemporal changes [29,30]. For a comprehensive review of studies using airborne LiDAR in geomorphology see [13] and references therein.

Several studies on (semi)automatic, object-based gully detection from airborne LiDAR have already been published. In the study of [26], a gully system in a forested area is investigated and gully morphologic information is extracted in a semi-manual procedure by looking at DTM-derived contour lines. They aim at deriving channel locations and network topological connectivity of the channels to improve channel-network maps and topological models. They conclude that the relatively low point density of terrain points and thus DTM resolution (2–4 m cell size) and, furthermore, occlusion of gully bottoms are the main limitations. This results in low mapping accuracy and poor morphological information. In [31] the authors derive gully maps in upland peatlands from airborne LiDAR DEMs with 2 m ground resolution. They identify gully areas through low difference from mean elevation (*i.e.*, high-pass filter) and high positive plan curvature. Their automated workflow can be applied to large areas. The achieved accuracy of gully width and depth are within the range of the horizontal and vertical accuracy of the input LiDAR data. The results of the raster-based approach of [32] highlight the need for adaptive thresholds for the detection of natural landforms such as channels and gullies. They use curvature and openness maps derived from a 1m-DTM from airborne LiDAR to identify the channel network via unsupervised channel pattern recognition and classification. A statistical approach is applied to derive optimum kernel sizes. The approach introduced by [33] detects gullies in airborne LiDAR data through surface curvature in multiple scales (*i.e.*, varying window sizes). Furthermore, they present an algorithm to connect fragmented parts to a gully network. Gaps in the network are due to eroded shallow parts in between.

Compared to the results derived from airborne LiDAR datasets, only a few studies have assessed the potential of ground-based LiDAR for gully investigation. The analysis of [18] is based on TLS point clouds as input to model gully cross-sections and to derive geometric parameters (e.g., cross-section area computation). Furthermore, they automatically extract the thalweg of a gully. They state the importance of data preprocessing, and identify TLS intensity correction (*cf.* [34]) and gully edge detection as future research topics. The study of [35] assesses the effect of TLS point sampling density on the characterization of ephemeral gullies within areas of agricultural land use. They outline guidance principles for multitemporal gully LiDAR surveys in order to minimize scanning effort while keeping the required topographic details as high as possible. The authors deploy the concept of semivariograms to quantitatively assess the relationship between LiDAR point density and topographic modeling. They conclude that, due to the inherent nature of heterogeneous point density distribution of TLS, there is a large potential to optimize scan settings and planning. In particular, data acquisition has to be regarded with respect to the (i) object of interest (e.g., scale, extent), (ii) detail of maintained micro-relief, and (iii) reduction of occlusion effects. One of the first comparisons of DEMs derived from terrestrial and airborne LiDAR for gully erosion estimation is presented by [36]. They stress the advantage of high point density of TLS and the preferable bird's eye view from airborne LiDAR to capture data even in deeply incised gullies, which is not possible with TLS due to topographic occlusion. Thus, both LiDAR data sources are complementary. They advise to capture the main gully system area-wide with high-resolution airborne LiDAR and, additionally, apply TLS in areas with narrow gully tributaries. Furthermore, they state that TLS is a suitable and cost-effective tool to develop time-series for monitoring of gully erosion processes.

To sum up, GIS-based geomorphological mapping of cushion peatlands using TLS data is not yet fully exploited. However, TLS has already proven a large potential to become a standard tool for

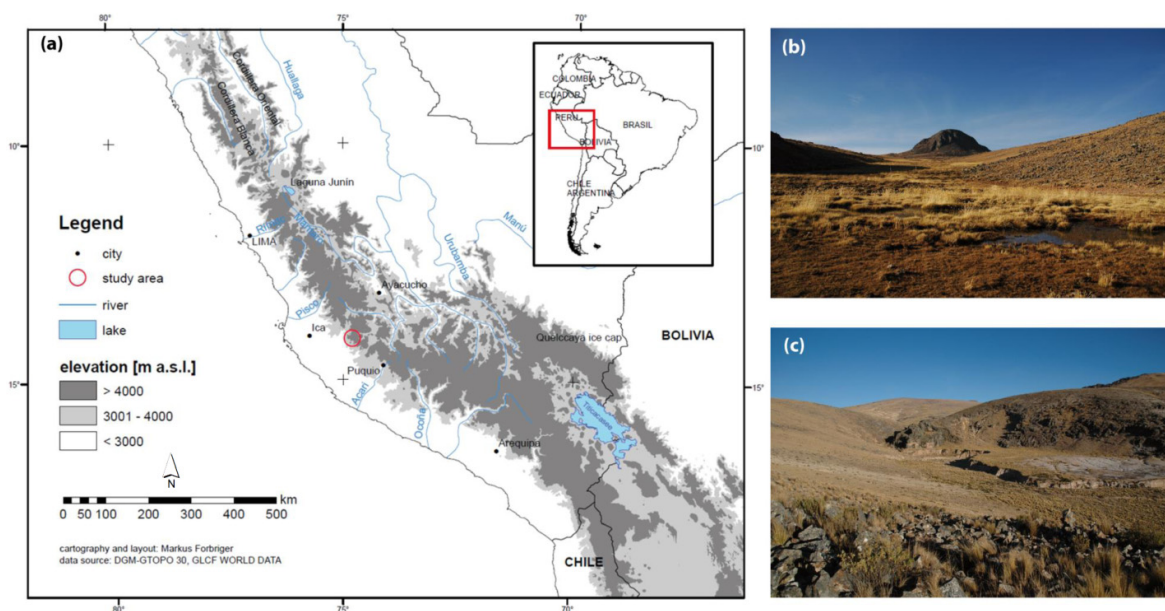
multitemporal monitoring of gully erosion. In particular the combination of DEMs from different data sources is increasingly gaining interest, such as airborne and terrestrial LiDAR as well as DTMs derived from images.

3. Study Area and Datasets

3.1. The Cerro Llamoca Study Site

The study area is located in the province of Lucanas in the western cordillera of the Peruvian Andes (Figure 1) in the catchment area of Río Viscas at the foot of Cerro Llamoca ($14^{\circ}10'S$, $74^{\circ}44'W$; 4,450 m a.s.l.). It belongs to the partly dry and humid Puna. This typical vegetation zone in the Andes is known for its particular harsh environmental conditions. The Puna is characterized by high diurnal temperature amplitudes, frequent frost, high solar radiation, low oxygen concentration, and water deficiency [2,4]. At the Cerro Llamoca an annual rainfall of about 200–400 mm per year is measured, from which 90% of the precipitation is during austral summer from November to March. Due to these conditions, only few plants grow in this vegetation zone. Cushion peatlands are highly adapted to the difficult environmental conditions and are mostly situated in this vegetation zone. Although they are neither dominated by sphagnum plants nor ombrogenous peats, they are peatlands. The longish extension of the Llamoca peatland can be subdivided in five parts: The upper and southern area are completely separated from the rest of the peatland and are entirely dried out due to strong erosion. The northern area and the lower part are only partly eroded and incised by gullies. The deep incision causes a drainage effect that leads to a lack of saturation in the exposed regions and, thus, to a change of the vegetation cover. However, the central area is the most intact part of the peatland due to fencing to protect it against grazing [4].

Figure 1. (a) Location of the study site in the Peruvian Andes ($14^{\circ}10'S$, $74^{\circ}44'W$). (b) and (c) pictures of the cushion peatland taken during a field trip in 2010.



The development of the Llamoca peatland is characterized through the alternation of periods of landscape stability with more humid climate and thus peat accumulation on the one hand, and phases of extreme events and thereby landscape destabilization on the other hand [4]. The latter had been responsible for the genesis of alluvial fans and sediment input. Nevertheless, cushion peatlands are able to recover from extreme events. However, anthropogenic influence decreases this ability so that erosion increasingly appears. Due to increased grazing, major changes in landscape stability have taken place. The reduction of vegetation in the proximity has great influence on the peat matrix, resulting in increased surface runoff and sediment flux [1]. Concentrated surface runoff incises gullies. This leads to a lower water level and thereby to a less saturated periphery of the peatland [4,10]. Through intensified grazing, the ecosystem loses the ability of regeneration and the auto-regulated processes of peat degradation are set off. Non-consolidated sediments at the peat surface are essential to initiate gully erosion in the Llamoca peatland.

3.2. LiDAR Datasets and Preprocessing

The supplied data was collected in August 2010, with the time-of-flight scanner Riegl VZ-400. The scanner operates with a narrow near-infrared (1,550 nm) laser beam with 0.3 mrad beam divergence (3 mm diameter at 10 m distance) providing up to 122,000 measurements per second. Range measurements of up to 400 m distance are possible. The maximum distance strongly depends on target reflectivity. The Riegl VZ-400 performs online echo detection where single echoes are derived from the waveform during data acquisition. The waveform capability of the system enables the separation of several echoes for each emitted laser shot. In this study all online-recorded echoes are used as input for further processing. The whole Llamoca peatland area of about 1.8 km² was captured with 46 scan positions and a total of 370 million single laser points (Figure 2).

Figure 2. LiDAR point cloud view of the cushion peatland and part of the gully system. The subfigure shows a cross-section through the point cloud and gives estimates of the depth and width dimensions.

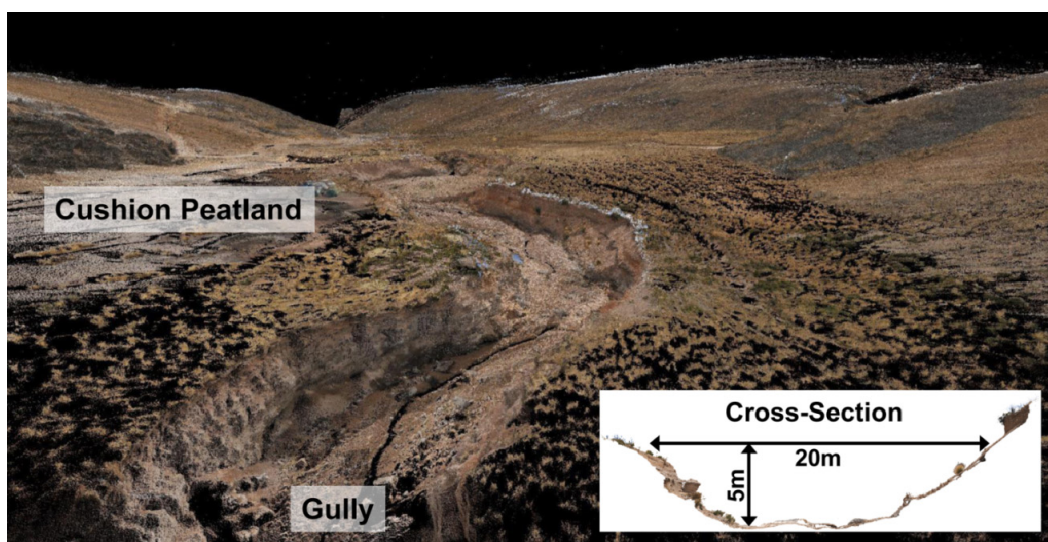
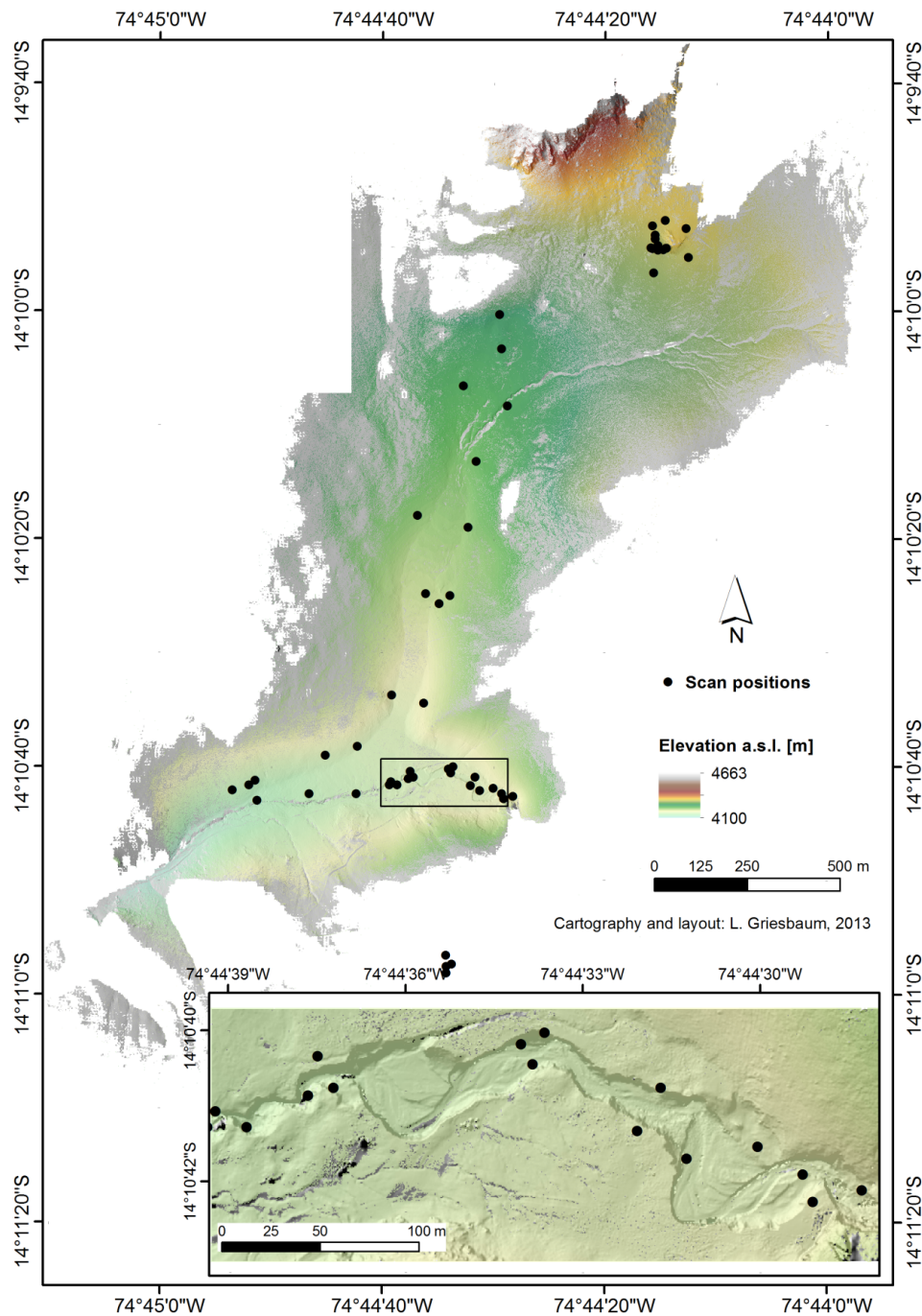


Figure 3. Scan positions and DTM with 0.5 m cell size derived from 370 million single point measurements shown as interpolated and filled shaded relief. The shaded DTM is superimposed and colored by elevation where cells contain recorded laser points. Thus, filled DTM cells are not colored by elevation in this map. The detailed zoom on the gully is outlined by a black rectangle in the shaded relief.



First, a coarse alignment of the scan positions is performed by matching cylindrical reflectors scanned with high resolution and by finding corresponding points between overlapping scan positions. For further refinement of the overall co-registration, the iterative closest point (ICP) algorithm within

the Multi-Station Adjustment (MSA) extension of the RiSCAN PRO software is applied [37]. The MSA reports an error (standard deviation) of 3.4 cm, which is sufficient for our gully detection analysis. Subsequent filtering and transformation into a DTM with 0.5 m cell size was performed using the LiDAR software OPALS [38]. The average point density in the central part of the gully system is 24 points/m². Areas close to scan positions or with overlapping data acquisition have significantly higher point densities, whereas areas in larger distance have much lower values. A cell size of 0.5 m is chosen to achieve a high number of cells over the entire study site containing laser point information. DTM generation includes (i) removal of outliers, (ii) derivation of a minimum height raster (0.5 m cell size), and (iii) filling of gaps in the minimum height raster by moving planes interpolation of the point cloud in a local neighborhood. For the interpolation of a cell value, the nearest 10 laser point neighbors are used, which are found in a search radius of 10 m. Cells already containing a minimum elevation value are not changed in order to maintain the highest topographic detail. Thus, only nodata cells are interpolated by local best fitting planes in each cell center. Larger gaps still occur on the hillslopes where larger depressions could not be seen by the LiDAR system. All other data gaps have been successfully interpolated during DTM generation (Figure 3).

4. Methods

The aim of our GIS-based workflow is to detect and delineate gully channels as polygons at individual gully scale. This will enable further detailed studies on gully erosion and fluvial morphological analysis by automatic geomorphometric parameter extraction of gully systems. The resolution of the input DTM with 0.5 m cell size is sufficient for gully mapping in the Cerro Llamoca peatland, as the study site's gullies clearly exceed 0.5 m in width. The main principle of the method is to parameterize a gully as a depression in the terrain surface (*i.e.*, loss of volume due to erosion), and additionally having a clear separation from the plateau depicted by a terrain discontinuity, *i.e.*, breakline (Figure 2). The outline of the gully polygon shall correspond to a certain upper boundary of the gully channel, such as the border between uneroded terrain and the incision.

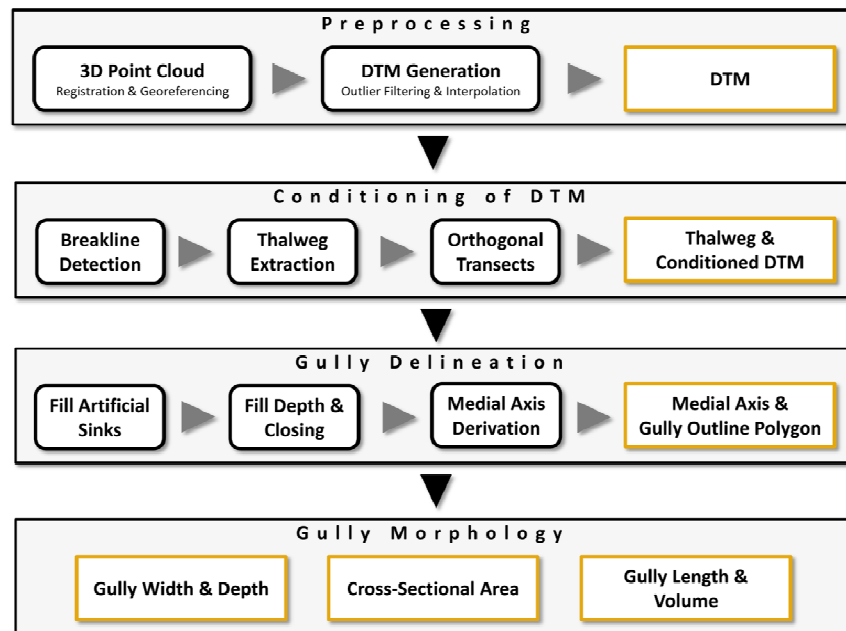
The chosen strategy is to make use of edge-based segmentation by breakline detection [20] combined with filling of sinks [39,40]. First, the upper breaklines of the gully incision are detected and serve as potential outline of the gully. In order to derive the gully as polygon, feature sink filling is performed on a conditioned DTM. For this purpose, the thalweg at the bottom of the gully is required and extracted from the DTM. Based on the thalweg, the gully system is divided into small patches by inserting artificial "dams" orthogonally to the gully thalweg along the gully course. Thereafter, both breaklines and small artificial dams at each patch are implemented into the DTM. This conditioned DTM is then used for sink filling of each "pool". The gully outline can be defined by using a threshold on fill depth for the artificially filled pools. The workflow is developed in GRASS GIS [41] and the main single steps are shown in Figure 4. Preprocessing and DTM generation have been described above in Section 3.2. The workflow is followed by a comparison with manually digitized reference data.

4.1. DTM Conditioning

Due to the nearly flat peat area and the steep gully slopes, the upper gully edges exhibit a high terrain curvature. Geomorphological breakline detection of upper gully edges is performed by the

method of [20], which is a curvature-based edge detection procedure. In this approach, a curvature raster is calculated by local surface approximation using a bivariate quadric function (*cf.* [42]). 3D breaklines can be derived by setting a threshold on high plan curvature and subsequent skeletonization of the masked areas.

Figure 4. Workflow of GIS-based gully delineation and geomorphometric parameter extraction.

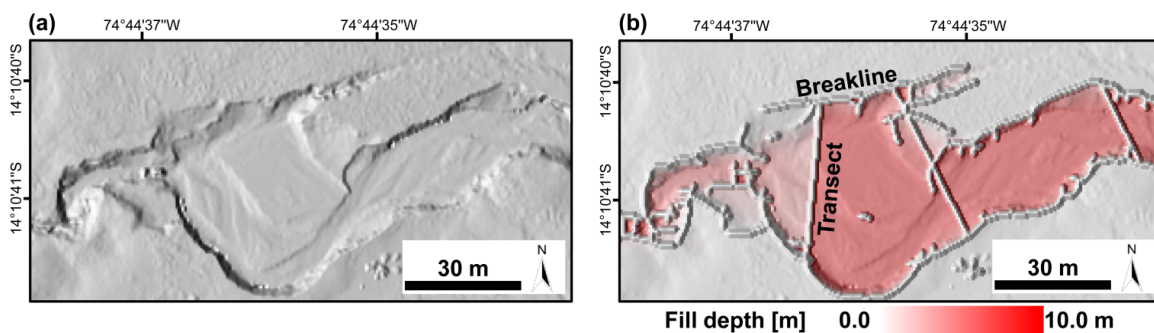


The thalweg is defined as the connecting line of the lowest points inside the gully along the channel course [43]. Several studies such as [31,32] assume concavity along the bottom of the gully, which does not hold for the Llamoca gullies with predominantly U-shaped erosion channels. The approach of [43] to extracting thalweg networks combines the morphological criteria of significant curvature (*i.e.*, discontinuous concave areas) and topographic convergence index. To generate the thalweg we use the topographic convergence index (TCI), which is defined as the logarithm of the ratio of flow accumulation and local slope [44]. Maximum TCI values describe regions with high chance for surface runoff. By masking areas with high TCI followed by skeletonization, the thalweg vector line is derived. In order to use the thalweg line for generating orthogonal transects, the vector line has to be smoothed to suppress effects of micro-topographic structures on the shape of the line. The final thalweg line is ready after applying vector line generalization by means of the Snakes algorithm [44].

Orthogonal transects, representing the artificial dams to construct pools along the gully channel, are constructed every 50 m with a lateral length of 40 m on each side of the thalweg. Shorter distances between transects should be chosen if the gully system has high elevation gradients along the channel in relation to the height step at the gully edges. In case of the Llamoca gully, the elevation changes within 50 m are much lower than the heights of the gully edges. To avoid transects to overlap neighboring gully channels, overhanging transect dangles at each side of the gully edges (*i.e.*, breaklines) are removed by intersecting the transect lines with the vectorized breaklines. In this step, only transects intersecting breaklines on both sides are trimmed automatically by keeping the middle transect part. All other transects keep their original length.

As the method of filling sinks considers multiple flow directions in the DTM, the raster breaklines and transect lines must be grown by one pixel in all directions to prevent the virtual surface water from overflowing. Both breaklines and thalweg transect lines are inserted as vertically extended objects into the DTM by adding a certain height to the DTM elevation (Figure 5). A height value is applied that definitely exceeds the maximum expected gully depth of the study area (here 10 m). This ensures that the sink-filling algorithm fills the whole gully volume and not only small local depressions at the gully bottom. Results of this processing step are the thalweg line and the modified DTM, which is used as input in the next step.

Figure 5. (a) Shading of original DTM. (b) Shading of modified DTM after insertion of breaklines and transects orthogonally to the thalweg by adding a constant height to the DTM elevations. The areas colored by fill depths indicate the artificial pools. Highest fill depth values are reached in sections that are completely encompassed by detected breaklines at the gully edges.



4.2. Gully Delineation

As outlined above, the DTM conditioned with artificial barriers serves as input for sink filling as implemented in GRASS GIS [40]. The conditioning of the DTM prior to sink filling has the advantage of providing distinct, detectable boundaries where the gully has clear edges. At the same time, due to the sink filling of the artificial gully pools, outlines can be derived even in areas where no clear edges are present. The artificially introduced sinks are filled up to the level of the sink spill point. In case of pools that are completely encompassed by breaklines and transects, the spill point corresponds to the location at the downstream orthogonal transect where the lowest gully channel elevation is present. In all other cases the spill point can be found at the gully edge with lowest elevation where no breakline was detected (Figure 5).

Subtracting the input DTM from the filled DTM leads to a raster of fill depth values. Masking areas with a fill depth above a certain threshold marks the main gully channel areas and depressions outside gullies. The fill depth values correspond to the elevation difference between spill point elevation and original DTM elevation. Depth values of gully sections that are completely encompassed by breaklines do not have a geomorphological meaning, as they are mainly related to the height of the artificial barriers. In case of “open” pools with missing artificial barriers at the edges, the fill depths are determined by the elevation of the lowest “open” gully edge. The two possible cases can be seen in Figure 5b.

The derived mask still contains the artificial barriers as holes between the single patches. By mathematical morphology of closing of the binary raster mask, these gaps are bridged and the patches along the gully channel are connected to the final gully polygons. Small isolated sinks can be removed by a threshold on polygon area (here $<10 \text{ m}^2$).

The medial axis of the gully is the closure of the set of points that have at least two closest points on the boundary (*cf.* [45]). It is derived from the gully polygon by applying the grassfire model. In this procedure the raster polygon area is thinned from all sides to a line with one pixel width. Resulting bifurcations are removed to derive the medial axis line vector. Analogous to the thalweg, the medial axis is smoothed for further application. The results of this step include the vector polygon of the gully areas and corresponding medial axes.

4.3. Gully Morphology

Descriptive geomorphometric parameters are necessary for understanding the erosion processes and the development of gullies in complex cushion peatland systems. The gully channel geometry is assessed and quantified through a series of cross-sections orthogonal to the medial axis [18]. The lengths of the orthogonal cross-sections and the distance between the cross-sections along the gully course have to be chosen in relation to the geomorphological characteristics of the study object. In our case the length of the cross-section is adapted automatically as it is determined and limited by the gully polygon. The shortest reasonable distance between the cross-sections is determined by the given resolution of the DTM. By draping the cross-sections over the LiDAR DTM, 3D lines are generated which are the input for assessing the width, depth and cross-sectional area along the gully channel course. Furthermore, summarizing the single cross-sections allows for calculating the overall eroded volume.

4.4. Comparison with Manual Reference Data

Automatic geomorphological mapping results may differ strongly from manual digitization. In order to compare and evaluate the proposed method, the approach of [20] is applied, where a rich reference dataset is produced through manual digitization based on shaded reliefs of the LiDAR DTM. The operators were asked to digitize the outline of the gully as polygon feature. Nine reference datasets are available. The automatic delineation is performed 6 times with varying fill depth thresholds of 0.5 m, 1.0 m, 1.5 m, 2.0 m, 2.5 m, and 3.0 m.

First, the statistics of area values of the automatically detected polygons is analyzed regarding the effect of different fill depth thresholds. Second, the area values of the manually digitized reference polygons are investigated regarding different interpreters. Third, the automatic extraction with a fill depth threshold of 0.5 m is compared and spatially intersected with the maximum (by spatial union) and minimum polygon (by spatial intersection) of all reference datasets.

5. Results and Discussion

This section gives detailed insight into the results of the developed methodology and discusses the findings of the study. As indicated in Figure 4, our approach comprises several results, which can be

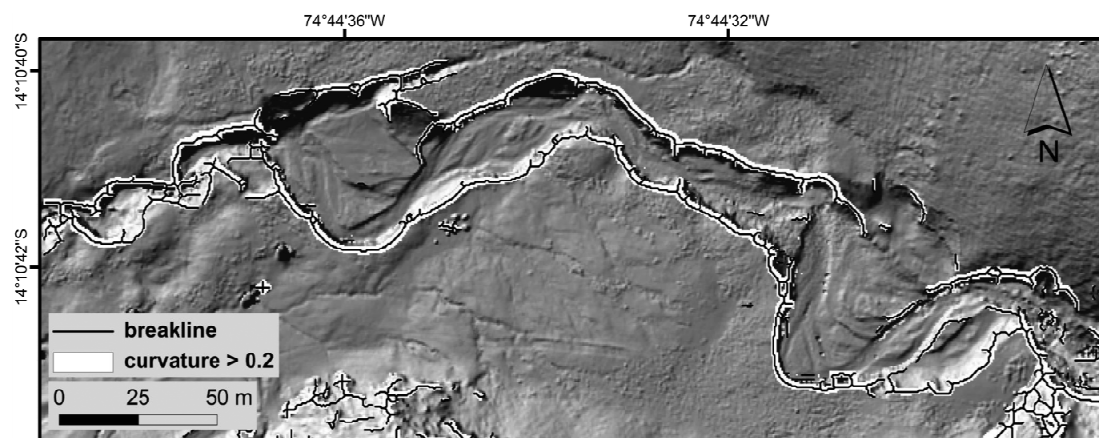
used directly for geomorphological quantification and interpretation. Additionally, they can be taken as input for further gully system analyses and simulations.

5.1. Gully Detection

The conditioning of the DTM implements breaklines and artificial dams orthogonally to the thalweg. The curvature-based breakline detection, already applied successfully to airborne LiDAR data [19,20], is able to detect distinct upper gully edges in the TLS DTM. In this step, a local window size of 9 by 9 cells and a curvature threshold of 0.2 have shown best results after manual testing of parameter combinations. In general, the optimum parameter set depends on gully shape (e.g., U-shaped) and the input DTM (e.g., resolution, scan geometry, and platform; [36]), and, thus, is site-specific. It is advisable to include an automatic threshold selection prior to breakline detection in case of transfer of the workflow to other study areas, data sources, gully characteristics, and so forth. This could be done by defining training edges and an accuracy metric to find optimal values [20].

The breakline detection outlines all convex surface discontinuities in the DTM (Figure 6). Due to the combination with sink filling, further breakline classification and removal are not required at this point. However, breaklines of gully incisions can easily be classified after gully detection using a distance threshold (e.g., buffer) between breakline and gully polygons.

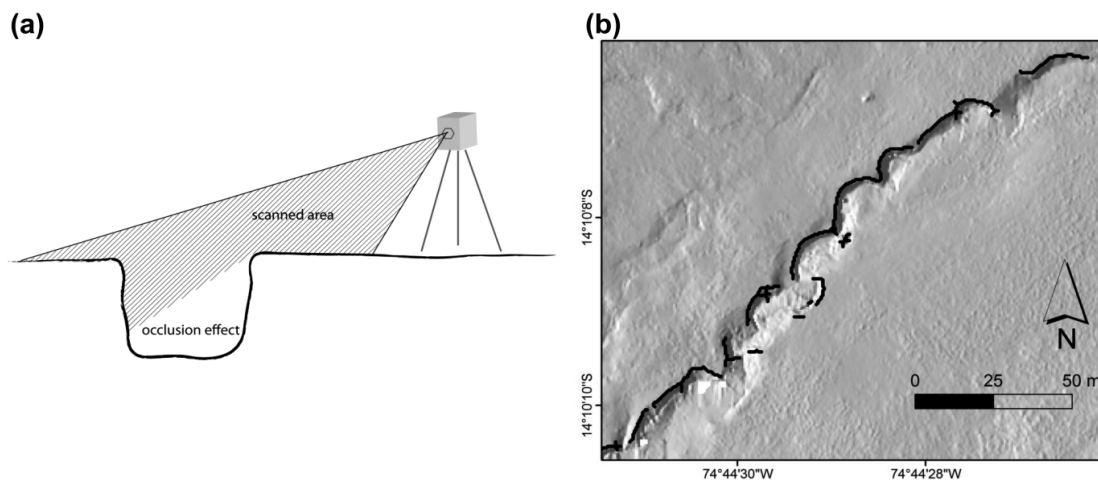
Figure 6. Breakline detection: Areas with high curvature are marked and resulting breaklines are shown. Not all parts of the gully are denoted by sharp edges and thus detected breaklines.



Breaklines are not found in areas where the gully has a smooth transition to the peatland plateau, as shown in Figure 6 in the northeastern part. Furthermore, breaklines cannot be detected in areas where the gully bottom has not been captured by the ground-based survey. Thus, the incision shape is not apparent in the DTM. In [14], it is stated that the DTM error is strongly influenced by the position of the scan locations relative to the morphology being surveyed. Additionally, the effect of occlusion has large impact on accuracy and morphological quality of the DTM, leading to data gaps that have to be interpolated in DTM generation [36]. Figure 7 highlights the effect of occlusion and shows detected breaklines in areas with interpolated data gaps. Our approach does not necessarily require breaklines on both sides of the gully channel. Although no complete elevation cross-profile of the incision is

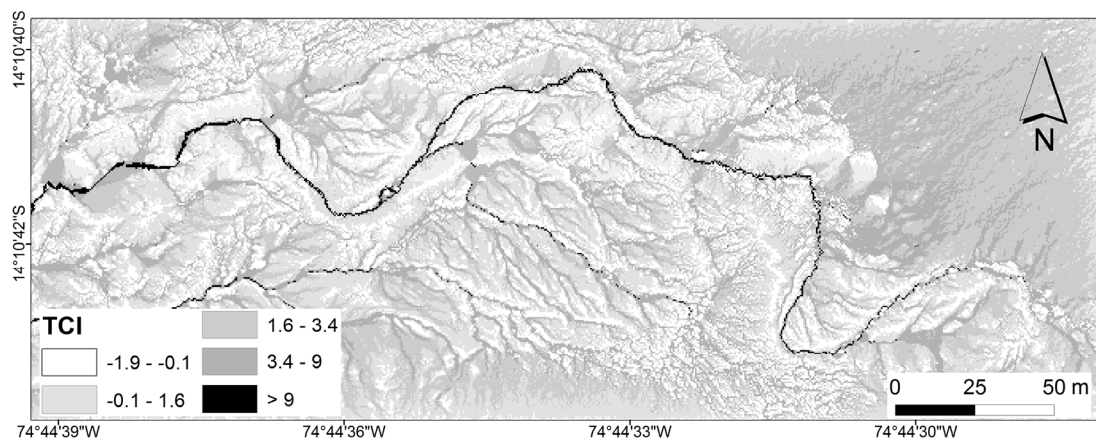
available, the gully outline detection succeeds due to the additional sink-filling step. However, too much missing gully channel information cannot be compensated by a detection approach relying on DTM information and leads to disconnected gully areas. The detected fragments need to be connected in a postprocessing step, such as in [33,43]. Data gaps are also caused by presence of water, which absorbs most of the near-infrared laser beams. Such laser shot dropouts could be modeled and used as additional input for gully detection [46].

Figure 7. (a) Occlusion effect in case of ground-based LiDAR leading to data gaps that have to be interpolated. (b) Missing gully shape information leads to smooth interpolated areas without distinct breaklines, e.g., on the southern side of the shown gully channel.



The thalweg detected by reclassifying the TCI serves as input for the implementation of the virtual orthogonal barriers. By reclassifying the TCI values and further processing (e.g., simplification) the thalweg can be extracted successfully in areas where the gully bottom morphology is present in the DTM. To limit the gully detection to the main channel system, a TCI threshold of >9 was assessed by visual inspection of the TCI raster (Figure 8).

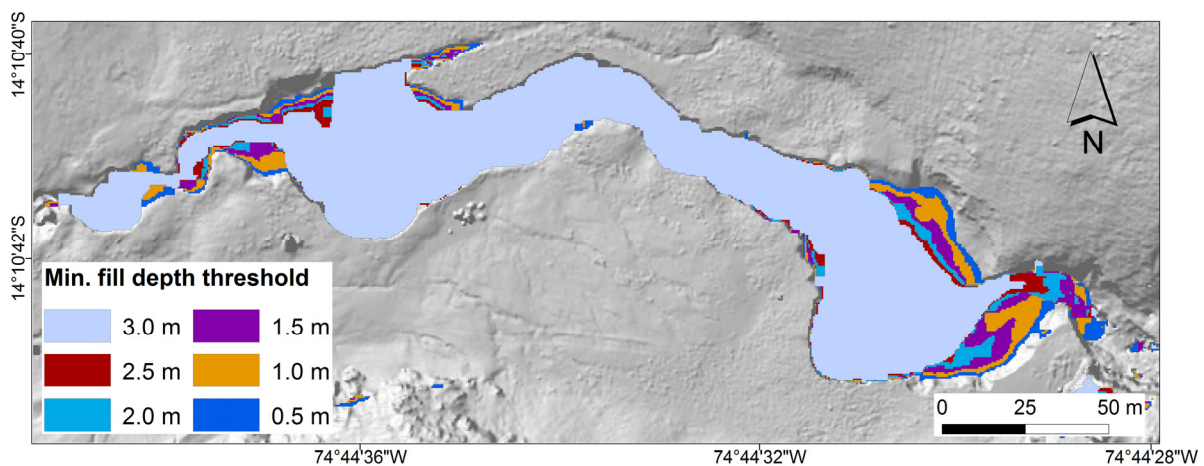
Figure 8. Topographic convergence index (TCI) raster for extracting the thalweg of the gully.



The gully outline polygon is clearly defined in areas with sharp edges and breaklines (*i.e.*, “closed” pools), whereas the sink filling determines the exterior outline in areas with smooth transitions between the gully bottom and the peatland plateau (*i.e.*, “open” pools). In these areas, the gully edge is not well defined by elevation and exhibits a certain fuzzy boundary zone. GIS-based mapping of distinct objects implies defined object boundaries. Our approach enables the derivation of fuzzy object outlines and to model smooth transitions by varying the minimum fill depth threshold. In case of high values for the threshold of fill depth, only the deeply incised gully parts are delineated leading to narrower gully polygons. At lower thresholds, and, thus, fill depth, the gullies are wider in areas without a clear jump in elevation at the edge. In case of “open” pools, the fill depth is determined by the elevation of the spill point at the gully boundary where no breaklines were detected. Thus, only gully areas below this elevation exhibit a fill depth above zero. The distance between the orthogonal transects has to be chosen with regard to the upstream elevation gradient of the upper gully edge and the gully bottom. In our study area a distance value of 50 m between the orthogonal transects is appropriate because the elevation changes of edge and gully bottom within a single artificial pool are smaller than the incision depth of the gully.

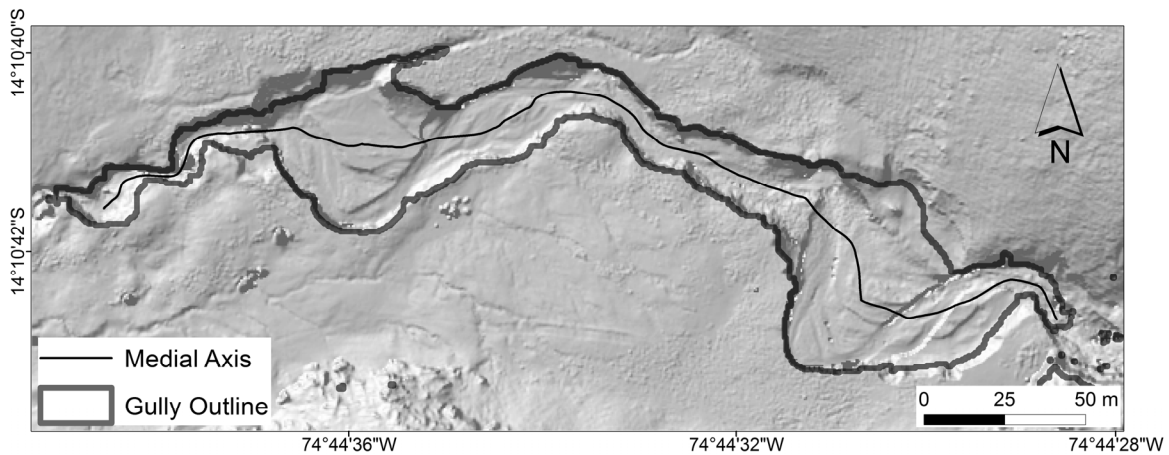
Figure 9 shows the sensitivity of the delineation approach in relation to the threshold on minimum fill depth and gully edge characteristics. Fuzzy boundaries can be recognized at the fluvial terraces in the eastern part of the gully, which were probably formed by various extreme events. In general, it can be stated that the selection of the appropriate threshold depends on the geomorphological research question and application (e.g., volume estimation or monitoring of gully edges).

Figure 9. Derived gully polygons with varying threshold on minimum fill depth after sink filling. Fuzzy gully outlines are present in areas with a smooth transition between channel and peatland plateau.



Based on the gully polygon the medial axis is derived (Figure 10). Although the medial axis has no geomorphological function, it is a valuable input for the following generation of cross-sections along the gully course.

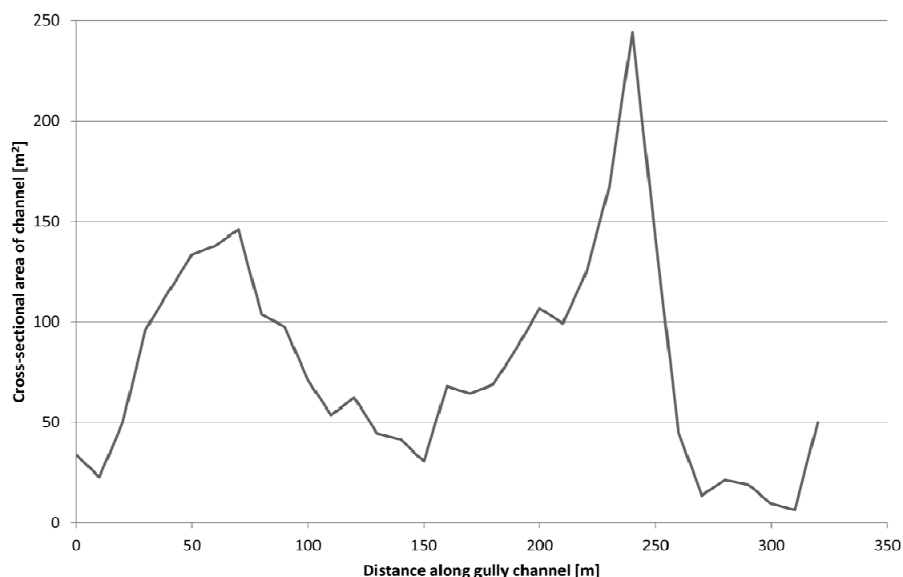
Figure 10. Medial axis of gully delineation using a minimum fill depth threshold of 0.5 m (cf. Figure 9). The medial axis from east to west is used as profile line for Figure 11.



5.2. Gully Morphology

Additionally to the gully channel area and length, information on variations in gully width, depth, cross-sectional area and thus volume along the course is provided by the developed workflow. The main gully system of the Llamoca peatland is characterized by significant variation of gully width. The values of width range between 3.5 m and 51 m. A similar variation can be observed for maximum gully depth varying from 2.4 m up to 7.5 m. Investigating width or cross-sectional area (Figure 11) together with slope gradient along the thalweg helps to identify vulnerable gully sections with higher probability of lateral and vertical erosion in case of extreme runoff events.

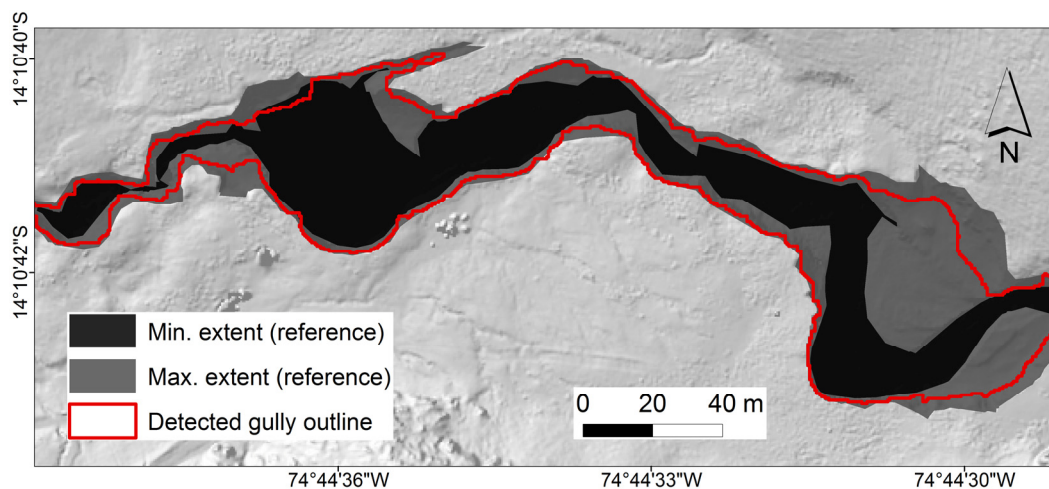
Figure 11. Profile of cross-sectional area sampled in 10-meter-distance intervals along a selected gully channel section. The profile line is taken along the medial axis shown in Figure 10.



5.3. Comparison with Manual Reference Data

The maximum and minimum extents of the nine manual reference outlines are displayed in Figure 12, together with an automatically extracted gully delineation. Already visually, one can clearly depict high correspondence of automatic extraction and reference in areas with well-defined edges. Distinct edges support manual mapping based on shaded reliefs as well as automatic delineation. In contrast, the areas with smooth transitions show high variation of the boundary locations in the reference datasets and in the six automatically extracted outlines using different fill depth thresholds (Figure 9).

Figure 12. Comparison of reference gully delineations with an automatic extraction (0.5 m depth threshold).



The gully polygon with minimum area is derived with the highest threshold (3 m) on depth and the maximum area with the lowest depth threshold (0.5 m). Looking at the descriptive statistics in Table 1, a lower variation in areal extent is present in the automatically derived polygons (8.6%) than in the manual reference datasets (13.0%). This is confirmed in the area of intersection of all polygons of each dataset stack, where the combined intersection of all manual references accounts for 62.8% of the mean polygon area, compared to 89% in the automatic extraction. The minimum area accounts only for 53% of the maximum area in the reference datasets. The minimum area of the automatic delineation exhibits almost 79% of the maximum polygon area. There is high correspondence between mean area value of automatic and manual extraction. The automatically extracted mean value reaches 92.5% of the manual area value.

The spatial comparison of the automatic extraction (fill depth threshold of 0.5 m) with the combined maximum (spatial union) and minimum (spatial intersection) polygon of the reference datasets reveals a high correspondence. Most of the automatically delineated area (99.8%) intersects with the maximum reference polygon, which can also be clearly seen in Figure 12. Almost the entire minimum reference polygon (99.5%) is covered by the automatic delineation. However, the automatic extraction covers only 79.7% of the maximum reference extent. Furthermore, it overestimates the gully area by a factor of 1.7 in relation to the minimum reference extent. From this evaluation it can be concluded that the automatic extraction corresponds very well to results derived by manual digitization and lies within the spatial boundaries of minimum and maximum extent of the reference polygons.

Table 1. Descriptive statistics of nine reference datasets and six automatically extracted gully polygons. The evaluation site is shown in Figure 12.

	Automatic Extraction	Manual Reference
No. of polygons	6	9
Min. polygon area [m ²]	6919	5284
Max. polygon area [m ²]	8773	9919
Mean polygon area [m ²]	7777	8411
Std. deviation polygon area [m ²]	665	1097
Coefficient of variation of area [%]	8.6	13.0
Min. area relative to max. area [%]	78.9	53.3
Area of spatial intersection of all polygons [m ²]	6919	5284
Area of spatial union of all polygons [m ²]	8773	10991

6. Conclusions and Future Work

Since gully erosion is a frequent phenomenon in highly sensitive ecosystems such as cushion peatlands, development of improved gully mapping methods and the derivation of geomorphometric parameters are essential. This paper presents the first study on automatic GIS and LiDAR-based detection and delineation of gully channels in a high altitude and remote cushion peatland in the Peruvian Andes.

The developed method uses a combination of breakline detection and sink filling based on a conditioned DTM. This is particularly beneficial in areas with smooth transitions and several small terraces depicting the border between gully channel and peatland plateau. Furthermore, the method can delineate channels even if gully bottoms have been captured only partly due to topographic occlusion of the laser scan. Fully occluded channel bottoms remain a challenge in terrestrial LiDAR data analysis, independently of the mapping method. The comparison of automatic gully extraction and manually digitized reference polygons reveals a high correspondence (93%) in polygon area values and in the spatial comparison derived by polygon intersection. The automatically derived gully delineation lies within the maximum and minimum digitized extents.

The introduced multi-step GIS workflow generates various results that can serve as input for multitemporal monitoring and gully system modeling. Results include the thalweg, medial axis, gully delineation and several geomorphometric channel parameters along the channel course (e.g., width, depth and cross-sectional area). In principle, the workflow can be transferred to other study areas and input DTMs with the necessity of tuning algorithm parameters and thresholds.

Future work will concentrate on the investigation of optimizing terrestrial LiDAR data acquisition for multitemporal gully channel monitoring by setting up guiding principles for field surveys. The impact of scan geometry, point sampling density and DTM resolution on gully delineation accuracy and morphometric parameters will be assessed. The full potential of TLS for cushion peatland studies is still underexploited. Radiometric backscatter values provided by full-waveform TLS offer promising complementary information to monitor geomorphology and also vegetation in cushion peatlands. Furthermore, future research should include the complementary advantages of multi-source 3D sensing, such as combining terrestrial LiDAR to capture steep slopes with airborne 3D data acquisition (e.g., UAV-based) in order to achieve a complete morphological shape of the objects of interest.

Acknowledgments

The authors cordially thank Martin Hämmerle, Kristina König, Fabian Schütt, Johannes Fuchs and Alexandra Laub for support in data processing and proofreading of the manuscript. This research was funded in part by the BMBF research project “Andean Transect—Climate Sensitivity of pre-Columbian Man-Environment-Systems”.

Conflicts of Interest

The authors declare no conflict of interest.

References and Notes

1. Valentin, C.; Poesen, J.; Li, Y. Gully erosion: Impacts, factors and control. *Catena* **2005**, *63*, 132–153.
2. Squeo, F.A.; Warner, B.G.; Aravena, R.; Espinoza, D. Bofedales: High altitude peatlands of the central Andes. *Revista Chilena de Historia Natural* **2006**, *79*, 245–255.
3. Alzérreca, H.; Laura, J.; Loza, F.; Lunda, D.; Ortega, J. Importance of Carrying Capacity of Sustainable Management of Key-andean Puna Rangelands (Bofedales) in Ulla Ulla, Bolivia. In *Land Use Change and Mountain Biodiversity*; Spehn, E., Liberman, M., Körner, C., Eds.; CRC Press, Taylor & Francis: Boca Raton, FL, USA, 2006; pp. 167–185.
4. Schitteck, K.; Forbriger, M.; Schäbitz, F.; Eitel, B. Cushion Peatlands—Fragile Water Resources in the High Andes of Southern Peru. In *Water—Contributions to Sustainable Supply and Use, Landscape and Sustainable Development*; Weingartner, H., Blumenstein, O., Vavelidis, M., Eds.; Workinggroup Landscape and Sustainable Development: Salzburg, Austria, 2012; pp. 63–84.
5. Marzloff, I.; Ries, J.B. Gully erosion monitoring in semi-arid landscapes. *Z. Geomorphol.* **2007**, *51*, 405–425.
6. Bocco, G. Gully erosion: Processes and models. *Prog. Phys. Geog.* **1991**, *15*, 392–406.
7. Morgan, R.P.C. *Soil erosion*. Longman: London, UK, New York, NY, USA, 1979; p. 113.
8. Evans, M.; Warburton, J.; Yang, J. Eroding blanket peat catchments: Global and local implications of upland organic sediment budgets. *Geomorphology* **2006**, *79*, 45–57.
9. Evans, M.; Warburton, J. *Geomorphology of Upland Peat: Erosion, Form and Landscape Change*; Wiley-Blackwell: West Sussex, UK, 2008.
10. Holden, J.; Gascoign, M.; Bosanko, N.R. Erosion and natural revegetation associated with surface land drains in upland peatlands. *Earth Surf. Process. Landforms* **2007**, *32*, 1547–1557.
11. Hancock, G.R.; Cawter, D.; Fityus, S.G.; Chandler, J.; Wells, T. The measurement and modelling of rill erosion at angle of repose slopes in mine spoil. *Earth Surf. Process. Landforms* **2008**, *33*, 1006–1020.
12. Hohenthal, J.; Alho, P.; Hyypä, J.; Hyypä, H. Laser scanning applications in fluvial studies. *Prog. Phys. Geog.* **2011**, *35*, 782–809.
13. Höfle, B.; Rutzinger, M. Topographic airborne LiDAR in geomorphology: A technological perspective. *Z. Geomorphol.* **2011**, *55*, 1–29.
14. Heritage, G.L.; Milan, D.J.; Large, A.R.G.; Fuller, I.C. Influence of survey strategy and interpolation model on DEM quality. *Geomorphology* **2009**, *112*, 334–344.

15. Heritage, G.L.; Hetherington, D. Towards a protocol for laser scanning in fluvial geomorphology. *Earth Surf. Process. Landforms* **2008**, *32*, 66–74.
16. Pirotti, F.; Guarnieri, A.; Vettore, A. Ground filtering and vegetation mapping using multi-return terrestrial laser scanning. *ISPRS J. Photogramm. Remote Sens.* **2013**, *76*, 56–63.
17. Castillo, C.; Pérez, R.; James, M.R.; Quinton, J.N.; Taguas, E.V.; Gómez, J.A. Comparing the Accuracy of Several Field Methods for Measuring Gully Erosion. *Soil Sci. Soc. Am. J.* **2011**, *76*, 1319–1332.
18. Momm, H.; Bingner, R.; Wells, R.; Dabney, S. Methods for Gully Characterization in Agricultural Croplands Using Ground-Based Light Detection and Ranging. In *Sediment Transport—Flow and Morphological Processes*; Bhuiyan, F., Ed.; InTech: Croatia, 2011. Available online: http://cdn.intechopen.com/pdfs/21752/InTech-Methods_for_gully_characterization_in_agricultural_croplands_using_ground_based_light_detection_and_ranging.pdf (accessed on 17 August 2013).
19. Rutzinger, M.; Höfle, B.; Vetter, M.; Pfeifer, N. Digital Terrain Models from Airborne Laser Scanning for the Automatic Extraction of Natural and Anthropogenic Linear Structures. In *Geomorphological Mapping*; Smith, M.J., Paron, P., Griffiths, J.S., Eds.; Elsevier: Oxford, UK, 2011; pp. 475–488.
20. Rutzinger, M.; Höfle, B.; Kringer, K. Accuracy of automatically extracted geomorphological breaklines from airborne LiDAR curvature images. *Geografiska. Annaler.: Series A, Phys. Geogr.* **2012**, *94*, 33–42.
21. Van Asselen, S.; Seijmonsbergen, A. Expert-driven semi-automated geomorphological mapping for a mountainous area using a laser DTM. *Geomorphology* **2006**, *78*, 309–320.
22. Poesen, J.; Nachtergaele, J.; Verstaeten, G.; Valentin, C. Gully erosion and environmental change: Importance and research needs. *Catena* **2003**, *50*, 91–133.
23. Marzolf, I.; Poesen, J. The potential of 3D gully monitoring with GIS using high-resolution aerial photography and a digital photogrammetry system. *Geomorphology* **2009**, *111*, 48–60.
24. Shruthi, R.B.; Kerle, N.; Jetten, V. Object-based gully feature extraction using high spatial resolution imagery. *Geomorphology* **2011**, *134*, 260–268.
25. D’Oleire-Oltmanns, S.; Eisank, C.; Drăgut, L.; Blaschke, T. An object-based workflow to extract landforms at multiple scales from two distinct data types. *IEEE Geosci. Remote Sens.* **2013**, *10*, 947–951.
26. James, L.A.; Watson, D.G.; Hansen, W.F. Using LiDAR data to map gullies and headwater streams under forest canopy: South Carolina, USA. *Catena* **2007**, *71*, 132–144.
27. Jones, A.F.; Brewer, P.A.; Johnstone, E.; Macklin, M.G. High-resolution interpretative geomorphological mapping of river valley environments using airborne LiDAR data. *Earth Surf. Process. Landforms* **2007**, *32*, 1574–1592.
28. Notebaert, B.; Verstraeten, G.; Govers, G.; Poesen, J. Qualitative and quantitative applications of LiDAR imagery in fluvial geomorphology. *Earth Surf. Process. Landforms* **2009**, *34*, 217–231.
29. Milan, D.J.; Heritage, G.L.; Hetherington, D. Application of a 3D laser scanner in the assessment of erosion and deposition volumes and channel change in a proglacial river. *Earth Surf. Process. Landforms* **2007**, *32*, 1657–1674.

30. Picco, L.; Mao, L.; Cavalli, M.; Buzzi, E.; Rainato, R.; Lenzi, M.A. Evaluating short-term morphological changes in a gravel-bed braided river using terrestrial laser scanner. *Geomorphology* **2013**, doi:10.1016/j.geomorph.2013.07.007.
31. Evans, M.; Lindsay, J. High resolution quantification of gully erosion in upland peatlands at the landscape scale. *Earth Surf. Process. Landforms* **2010**, *35*, 876–886.
32. Sofia, G.; Tarolli, P.; Cazorzi, F.; Dalla Fontana, G. An objective approach for feature extraction: distribution analysis and statistical descriptors for scale choice and channel network identification. *Hydrol. Earth Syst. Sci.* **2011**, *15*, 1387–1402.
33. Baruch, A.; Filin, S. Detection of gullies in roughly textured terrain using airborne laser scanning data. *ISPRS J. Photogramm. Remote Sens.* **2011**, *66*, 564–578.
34. Höfle, B. Radiometric correction of terrestrial LiDAR point cloud data for individual maize plant detection. *IEEE Geosci. Remote Sens.* **2013**, doi:10.1109/LGRS.2013.2247022.
35. Momm, H.G.; Binger, R.L.; Wells, R.R.; Dabney, S.M.; Frees, L.D. Effect of terrestrial LiDAR point sampling density in ephemeral gully characterization. *Open J. Mod. Hydrol.* **2013**, *3*, 38–49.
36. Perroy, R.L.; Bookhagen, B.; Asner, G.P.; Chadwick, O.A. Comparison of gully erosion estimates using airborne and ground-based LiDAR on Santa Cruz Island, California. *Geomorphology* **2010**, *118*, 288–300.
37. Riegl. Available online: <http://www.riegl.com> (accessed on 16 August 2013).
38. Pfeifer, N.; Mandlbürger, G.; Otepka, J.; Karel, W. OPALS—A framework for Airborne Laser Scanning data analysis. *Comput. Environ. Urban.* **2013**, in press.
39. Arge, L.; Chase, J.S.; Halpin, P.N.; Toma, L.; Vitter, J.S.; Urban, D.; Wickremesinghe, R. Flow computation on massive grid terrains. *GeoInformatica* **2003**, *7*, 283–313.
40. Metz, M.; Mitasova, H.; Harmon, R.S. Efficient extraction of drainage networks from massive, radar-based elevation models with least cost path search. *Hydrol. Earth Syst. Sci.* **2011**, *15*, 667–678.
41. Neteler, M.; Bowman, M.H.; Landa, M.; Metz, M. GRASS GIS: A multi-purpose open source GIS. *Environ. Model. Softw.* **2012**, *31*, 124–130.
42. Wood, J. The Geomorphological Characterisation of Digital Elevation Models. Ph.D. Dissertation, University of Leicester, Leicester, UK, 1996.
43. Thommeret, N.; Bailly, J.S.; Puech, C. Extraction of thalweg networks from DTMs: Application to badlands. *Hydrol. Earth Syst. Sci.* **2010**, *14*, 1527–1536.
44. GRASS Development Team—GRASS GIS 6.4.3 Reference Manual. Available online: http://grass.fbk.eu/grass64/manuals/html64_user/index.html (accessed on 9 June 2012).
45. Karimipour, F.; Ghandehari, M.; Ledoux, H. Watershed delineation from the medial axis of river networks. *Comput. Geosci.* **2013**, *59*, 132–147.
46. Höfle, B.; Vetter, M.; Pfeifer, N.; Mandlbürger, G.; Stötter, J. Water surface mapping from airborne laser scanning using signal intensity and elevation data. *Earth Surf. Process. Landforms* **2009**, *34*, 1635–1649.